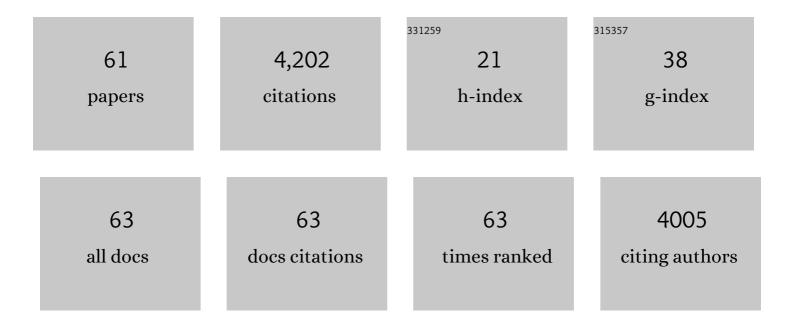
List of Publications by Year in descending order

Source: https://exaly.com/author-pdf/11235782/publications.pdf Version: 2024-02-01



#	Article	IF	CITATIONS
1	Retinal Imaging and Image Analysis. IEEE Reviews in Biomedical Engineering, 2010, 3, 169-208.	13.1	1,021
2	Intraretinal Layer Segmentation of Macular Optical Coherence Tomography Images Using Optimal 3-D Graph Search. IEEE Transactions on Medical Imaging, 2008, 27, 1495-1505.	5.4	300
3	Decreased Retinal Ganglion Cell Layer Thickness in Patients with Type 1 Diabetes. , 2010, 51, 3660.		294
4	Early Neurodegeneration in the Retina of Type 2 Diabetic Patients. , 2012, 53, 2715.		273
5	Three-Dimensional Analysis of Retinal Layer Texture: Identification of Fluid-Filled Regions in SD-OCT of the Macula. IEEE Transactions on Medical Imaging, 2010, 29, 1321-1330.	5.4	186
6	Effect of Age on Individual Retinal Layer Thickness in Normal Eyes as Measured With Spectral-Domain Optical Coherence Tomography. , 2013, 54, 4934.		157
7	Splat Feature Classification With Application to Retinal Hemorrhage Detection in Fundus Images. IEEE Transactions on Medical Imaging, 2013, 32, 364-375.	5.4	147
8	Segmentation of the Optic Disc in 3-D OCT Scans of the Optic Nerve Head. IEEE Transactions on Medical Imaging, 2010, 29, 159-168.	5.4	144
9	Association of visual function and ganglion cell layer thickness in patients with diabetes mellitus type 1 and no or minimal diabetic retinopathy. Vision Research, 2011, 51, 224-228.	0.7	110
10	Optimal Multiple Surface Segmentation With Shape and Context Priors. IEEE Transactions on Medical Imaging, 2013, 32, 376-386.	5.4	99
11	Vessel Boundary Delineation on Fundus Images Using Graph-Based Approach. IEEE Transactions on Medical Imaging, 2011, 30, 1184-1191.	5.4	93
12	Automated Segmentation of the Cup and Rim from Spectral Domain OCT of the Optic Nerve Head. , 2009, 50, 5778.		82
13	Automated Segmentation of Neural Canal Opening and Optic Cup in 3D Spectral Optical Coherence Tomography Volumes of the Optic Nerve Head. , 2010, 51, 5708.		79
14	Automated Quantification of Volumetric Optic Disc Swelling in Papilledema Using Spectral-Domain Optical Coherence Tomography. , 2012, 53, 4069.		77
15	Retinal ganglion cell layer thinning within one month of presentation for optic neuritis. Multiple Sclerosis Journal, 2016, 22, 641-648.	1.4	77
16	Causes and Prognosis of Visual Acuity Loss at the Time of Initial Presentation in Idiopathic Intracranial Hypertension. , 2015, 56, 3850.		70
17	Automated 3-D method for the correction of axial artifacts in spectral-domain optical coherence tomography images. Biomedical Optics Express, 2011, 2, 2403.	1.5	67
18	Automated Method for Identification and Artery-Venous Classification of Vessel Trees in Retinal Vessel Networks. PLoS ONE, 2014, 9, e88061.	1.1	66

#	Article	IF	CITATIONS
19	Multimodal Segmentation of Optic Disc and Cup From SD-OCT and Color Fundus Photographs Using a Machine-Learning Graph-Based Approach. IEEE Transactions on Medical Imaging, 2015, 34, 1854-1866.	5.4	62
20	Vessel segmentation in 3D spectral OCT scans of the retina. , 2008, , .		46
21	A combined machine-learning and graph-based framework for the segmentation of retinal surfaces in SD-OCT volumes. Biomedical Optics Express, 2013, 4, 2712.	1.5	46
22	Multimodal Retinal Vessel Segmentation From Spectral-Domain Optical Coherence Tomography and Fundus Photography. IEEE Transactions on Medical Imaging, 2012, 31, 1900-1911.	5.4	43
23	Relationships of Retinal Structure and Humphrey 24-2 Visual Field Thresholds in Patients With Glaucoma. Investigative Ophthalmology and Visual Science, 2015, 56, 259-271.	3.3	43
24	Retinal Ganglion Cell Layer Thinning Within One Month of Presentation for Non-Arteritic Anterior Ischemic Optic Neuropathy. , 2016, 57, 3588.		37
25	Automated construction of arterial and venous trees in retinal images. Journal of Medical Imaging, 2015, 2, 044001.	0.8	35
26	Robust Multiscale Stereo Matching from Fundus Images with Radiometric Differences. IEEE Transactions on Pattern Analysis and Machine Intelligence, 2011, 33, 2245-2258.	9.7	34
27	Optical Coherence Tomography Analysis Based Prediction of Humphrey 24-2 Visual Field Thresholds in Patients With Glaucoma. , 2017, 58, 3975.		34
28	Registration of 3D spectral OCT volumes using 3D SIFT feature point matching. Proceedings of SPIE, 2009, , .	0.8	29
29	Peripapillary Retinal Pigment Epithelium Layer Shape Changes From Acetazolamide Treatment in the Idiopathic Intracranial Hypertension Treatment Trial. , 2017, 58, 2554.		29
30	A machine-learning graph-based approach for 3D segmentation of Bruch's membrane opening from glaucomatous SD-OCT volumes. Medical Image Analysis, 2017, 39, 206-217.	7.0	28
31	RetFM-J, an ImageJ-based module for automated counting andÂquantifying features of nuclei in retinal whole-mounts. Experimental Eye Research, 2016, 146, 386-392.	1.2	24
32	Distribution of Damage to the Entire Retinal Ganglion Cell Pathway. JAMA Ophthalmology, 2012, 130, 1118.	2.6	23
33	Quantitative measurement of retinal ganglion cell populations via histology-based random forest classification. Experimental Eye Research, 2016, 146, 370-385.	1.2	23
34	Reproducibility of SD-OCT–Based Ganglion Cell–Layer Thickness in Glaucoma Using Two Different Segmentation Algorithms. , 2013, 54, 6998.		22
35	Automated Detection of Malarial Retinopathy-Associated Retinal Hemorrhages. , 2012, 53, 6582.		21
36	Multimodal registration of SD-OCT volumes and fundus photographs using histograms of oriented gradients. Biomedical Optics Express, 2016, 7, 5252.	1.5	21

#	Article	IF	CITATIONS
37	Automated 3D segmentation of intraretinal layers from optic nerve head optical coherence tomography images. Proceedings of SPIE, 2010, , .	0.8	20
38	2-D Pattern of Nerve Fiber Bundles in Glaucoma Emerging from Spectral-Domain Optical Coherence Tomography. , 2012, 53, 483.		20
39	Automated segmentation of the optic disc margin in 3-D optical coherence tomography images using a graph-theoretic approach. Proceedings of SPIE, 2009, , .	0.8	18
40	Quantitative Evaluation of Papilledema from Stereoscopic Color Fundus Photographs. , 2012, 53, 4490.		18
41	Automated Segmentation of 3-D Spectral OCT Retinal Blood Vessels by Neural Canal Opening False Positive Suppression. Lecture Notes in Computer Science, 2010, 13, 33-40.	1.0	18
42	Incorporation of gradient vector flow field in a multimodal graph-theoretic approach for segmenting the internal limiting membrane from glaucomatous optic nerve head-centered SD-OCT volumes. Computerized Medical Imaging and Graphics, 2017, 55, 87-94.	3.5	16
43	Automated 3D Segmentation of Multiple Surfaces with a Shared Hole: Segmentation of the Neural Canal Opening in SD-OCT Volumes. Lecture Notes in Computer Science, 2014, 17, 739-746.	1.0	16
44	Automated 3D Segmentation of Intraretinal Surfaces in SD-OCT Volumes in Normal and Diabetic Mice. Translational Vision Science and Technology, 2014, 3, 8.	1.1	15
45	Identification and reconnection of interrupted vessels in retinal vessel segmentation. , $2011,$, .		13
46	The Pattern of Visual Fixation Eccentricity and Instability in Optic Neuropathy and Its Spatial Relationship to Retinal Ganglion Cell Layer Thickness. , 2016, 57, OCT429.		13
47	Automated method for the identification and analysis of vascular tree structures in retinal vessel network. Proceedings of SPIE, 2011, , .	0.8	12
48	AxonDeep: Automated Optic Nerve Axon Segmentation in Mice With Deep Learning. Translational Vision Science and Technology, 2021, 10, 22.	1.1	11
49	Automated artery-venous classification of retinal blood vessels based on structural mapping method. Proceedings of SPIE, 2012, , .	0.8	10
50	Registration of 3D spectral OCT volumes combining ICP with a graph-based approach. , 2012, , .		10
51	A Deep-Learning Approach for Automated OCT En-Face Retinal Vessel Segmentation in Cases of Optic Disc Swelling Using Multiple En-Face Images as Input. Translational Vision Science and Technology, 2020, 9, 17.	1.1	9
52	Multimodal segmentation of optic disc and cup from stereo fundus and SD-OCT images. Proceedings of SPIE, 2013, , .	0.8	8
53	Incorporation of texture-based features in optimal graph-theoretic approach with application to the 3D segmentation of intraretinal surfaces in SD-OCT volumes. , 2012, , .		7
54	Temporal Relationship Between Visual Field, Retinal and Microvascular Pathology Following		7

4 ¹²⁵I-Plaque Brachytherapy for Uveal Melanoma., 2021, 62, 3.

#	Article	IF	CITATIONS
55	Utility of Spectral-Domain Optical Coherence Tomography in Differentiating Papilledema From Pseudopapilledema: A Prospective Longitudinal Study. Journal of Neuro-Ophthalmology, 2021, 41, e509-e515.	0.4	5
56	The Effect of Acetazolamide and Weight Loss on Intraocular Pressure in Idiopathic Intracranial Hypertension Patients. Journal of Glaucoma, 2019, 28, 352-356.	0.8	4
57	A Method for an Image-Analysis-Based Two-Dimensional Computational Fluid Dynamics Simulation of Moving Fish. Transactions of the American Fisheries Society, 2012, 141, 185-198.	0.6	3
58	Movement of Retinal Vessels to Optic Nerve Head with Intraocular Pressure Elevation in a Child. Ophthalmology, 2015, 122, 1532-1534.	2.5	3
59	Extending the XNAT archive tool for image and analysis management in ophthalmology research. Proceedings of SPIE, 2013, , .	0.8	0
60	Incorporation of learned shape priors into a graph-theoretic approach with application to the 3D segmentation of intraretinal surfaces in SD-OCT volumes of mice. Proceedings of SPIE, 2014, , .	0.8	0
61	Graph Algorithmic Techniques for Biomedical Image Segmentation. , 2014, , 3-45.		Ο